Inferring fluid volume during earthquake swarms using seismic catalogues

Philippe Danré, Louis De Barros, Frédéric Cappa

Geophysical Journal International

Geophys. J. Int. (2023) **232,** 829–841
Advance Access publication 2022 September 13
GJI Seismology

https://doi.org/10.1093/gji/ggac345

Inferring fluid volume during earthquake swarms using seismic catalogues

Philippe Danré [1], Louis De Barros[1] and Frédéric Cappa[1,2]

[1] *Université Côte d'Azur, CNRS, Observatoire de la Côte d'Azur, IRD, Géoazur, 250 rue Albert Einstein, Sophia Antipolis 06560 Valbonne, France. E-mail: danre@geoazur.unice.fr*
[2] *Institut Universitaire de France, Paris, France*

Accepted 2022 August 25. Received 2022 August 23; in original form 2022 May 5

SUMMARY

Many studies have pointed out a correlation between either the cumulative or the maximum seismic moment and the injected fluid volume when analysing global data sets of fluid injection-induced earthquake sequences. However, those correlations become quite uncertain when looking at individual episodes, mainly because of the large aseismic component of the induced deformation. If natural swarms are thought to result from the same physical processes as sequences from anthropogenic origin, little is still known about them as observations are limited by the depth of the active zone and the moderate deformations. In this work, we make profit of the similarity between both natural and injection-induced swarms. To this aim, we develop new relations between seismic observables and hydraulic attributes by using a global compilation of injection-induced earthquake catalogues, leading to two methods to estimate the injected fluid volume based solely on earthquake catalogues. Once the precision of our approaches is validated, we estimate the volume and flowrate of fluids circulating in diverse natural swarms, shedding a new light on the fluid dynamics that trigger them.

Key words: Earthquake dynamics; Induced seismicity; Statistical seismology.

1 INTRODUCTION

1.1 Relating seismicity to injected fluid volume

Earthquake swarms are episodes of clustered seismicity, in time and space, with no clear main shock having a much larger magnitude than the other events. Those seismic sequences are found in a diversity of geological contexts, such as in mountain ranges (Ide 2001; Jenatton *et al.* 2007), near transform faults (Roland & McGuire 2009), near volcanoes (White & McCausland 2016; Shelly & Hardebeck 2019; Li *et al.* 2021) and in extensional zones (Fischer *et al.* 2014; De Barros *et al.* 2020). Swarm activity is generally steadily growing and then decreasing, but quite important events can occur during those sequences, like the $M_w = 4.4$ earthquake during the 4 year-long Cahuilla swarm (Ross *et al.* 2020). Large earthquakes may also follow a swarm activity like the $M_w = 6.3$ L'Aquila earthquake in Italy in 2009 (Di Luccio *et al.* 2010).

The development of anthropogenic fluid injections at depth (Ellsworth 2013), for geothermal projects (Kraft & Deichmann 2014; Kwiatek *et al.* 2019), for hydraulic fracturing in shale formations (Eaton & Schultz 2018) or wastewater disposal (Goebel *et al.* 2016) has shown that injections at depth also induce sequences of clustered seismicity (Fig. 1a).The relation between fluid injection and seismicity has been investigated for decades, as it is of great interest in understanding the physics of earthquakes and for improved mitigation of seismic risks associated with large-scale geo-energy projects (McGarr 1976; Giardini 2009; Van der Elst *et al.* 2016; Galis *et al.* 2017). Assuming that fluid is injected into fully saturated porous rocks, McGarr (1976, 2014) linked the injected volume V_{inj} to the cumulated seismic moment $M_{0,seismic}$ by a simple relation $M_{0,seismic} = 2{*}G{*}V_{inj}$ (Fig. 1b), with G being the rock shear modulus. Using fracture mechanics theory, Galis *et al.* (2017) showed that the maximum seismic moment of self-arrested ruptures scales with the injected fluid volume; and based on statistical methods, van der Elst *et al.* (2016) demonstrated that the total number of earthquakes is controlled by the injected fluid volume. Also, during an injection, the seismic moment ($M_{0,seismic}$) is observed to grow with the injected fluid volume ($V_{inj,}$ Fig. 1c, Bentz *et al.* 2020). However, such a correlation remains limited as it only represents an upper bound for most of the swarms, leading to the inequality $M_{0,seismic} \leq 2{*}G{*}V_{inj}$ (McGarr & Barbour 2018; Figs 1b and c).

Recently, studies have shown that the discrepancy between observations and the McGarr's law (2014) can be explained by the fact that a part of the fluid-induced deformation is aseismic, filling the gap between the observed seismic moment and its expected value (McGarr & Barbour 2018; De Barros *et al.* 2019). Indeed, aseismic slip has been observed in both laboratory experiments (Goodfellow *et al.* 2015; Wang *et al.* 2020), field experiments (Guglielmi *et al.* 2015; Duboeuf *et al.* 2017), during reservoir stimulations (Schmittbuhl *et al.* 2014; Wei *et al.* 2015; Eyre *et al.* 2019;

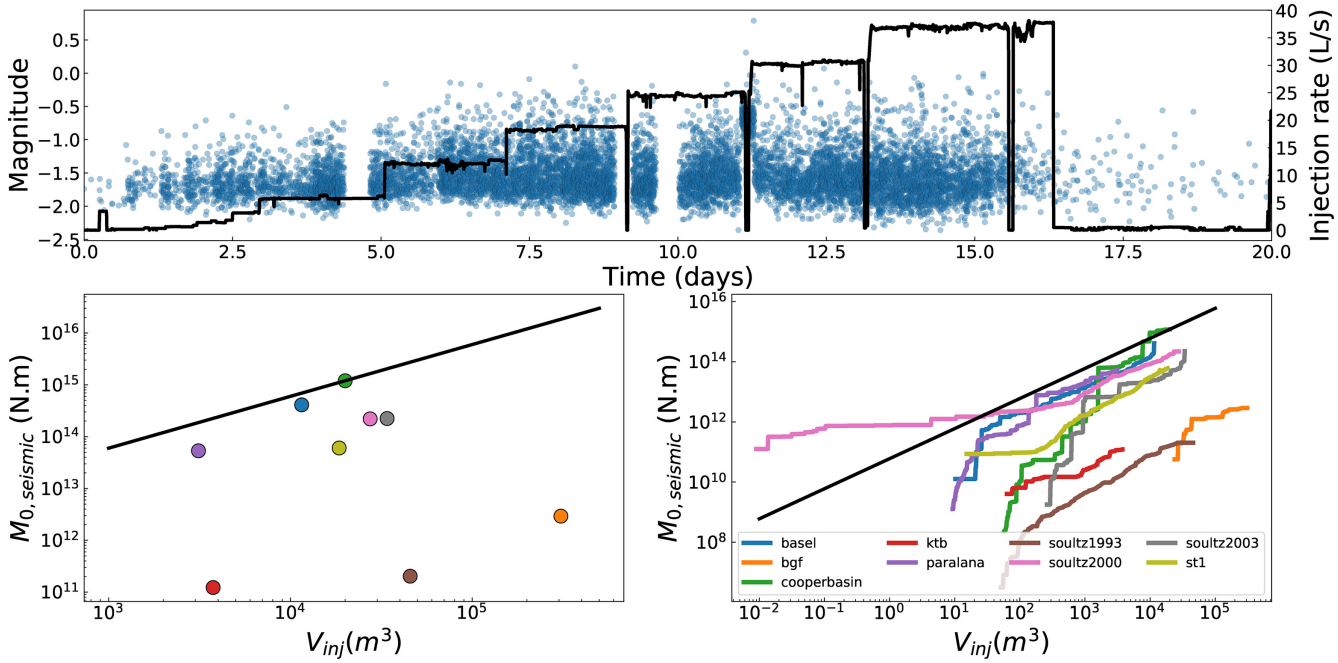

Figure 1. (a) Injection rate (L s^{-1}) and magnitudes of induced earthquakes occurring during the 1993 Soultz-Sous-Forets (Eastern France) injection sequence for geothermal exploitation. (b) Total seismic moment (N.m) as a function of the total injected fluid volume (m^3) for a variety of injection-induced sequences. Data are from Bentz *et al.* 2020. Black line represents the expected value following $M_{0,\text{seismic}} = 2GV_{\text{inj}}$ with $G = 30$ GPa. (C) Growth of cumulative seismic moment with the injected fluid volume, from the same data set.

Eyre *et al.* 2022) as well as in numerical simulations (Wynants-Morel *et al.* 2020; Yang & Dunham 2021). However, its quantification remains difficult as the measurement methods are limited by the weak deformations caused by the injections, their depth and durations. Relating injected fluid volume to deformation therefore requires other relations than those already available in the literature, in order to take into account the contribution of aseismic slip.

1.2 Natural earthquake swarms are also fluid-induced sequences

For a few decades, new findings have highlighted similarities between injection-induced and natural swarms. Most of the swarms observed in the upper crust, outside subduction areas, are thought to be primarily driven by fluid processes. Indeed, seismicity migration is generally observed in natural earthquake swarms, with diffusion-like migration (Parotidis *et al.* 2003; Chen *et al.* 2012) or more complex hydromechanical features (De Barros *et al.* 2020, 2021). It is also a general feature of injection-induced sequences (Shapiro *et al.* 1997; Goebel & Brodsky 2018). Other evidence supports the idea that natural and injection-induced earthquake swarms are caused by the same physical processes, like a weak moment release compared to the spatial extent of the swarms (Fischer & Hainzl 2017, 2021). Duration, migration velocity and moment released during injection-induced and natural sequences scale in a similar way (Danre *et al.* 2021). By analogy with studies of injection-induced sequences, fluid diffusion and aseismic slip are therefore thought to play a key role in natural swarms. Particularly, the knowledge of the fluid volume acting in those sequences is crucial to understand the swarm dynamics and associated hazards. At depth, however, geophysical information regarding fluids and aseismic slip are often not known making the estimation of fluid volume difficult to quantify and poorly constrained for natural swarms.

Here, we develop new relations between injected fluid volume and seismic observables, for injection-induced earthquake swarms. Our objective is then to apply those relations on natural earthquake swarms in order to reconstruct involved fluid volume that is unknown at such kilometres depths. To do that, we calibrate our approaches on nine earthquake catalogues of injection-induced sequences. We compute the aseismic moment released during those swarms by analogy with creep studies investigating the aseismic loading of seismic asperities (Uchida 2019), and relate this estimate to the injected fluid volume. We also show that two parameters used for earthquake swarms studies, the effective stress drop and the seismogenic index, are strongly correlated, leading to a new empirical relation between injected fluid volume and seismic observables. Finally, after comparing the estimated volumes for the two methods with the actual injected volume values, we use our findings to estimate the volume of fluids circulating during nine natural swarms based solely on earthquake catalogues.

2 EARTHQUAKES CATALOGUES

For this study, we used 18 well-documented earthquake catalogues, including nine injection-induced sequences and nine natural swarms (Fig. 2, see Supporting Information for a complete description). For simplicity, we selected cases of injection-induced seismicity with a single injection borehole interval rather than sites with multiple injections occurring at the same time. For natural swarms, we chose sequences for which fluid involvement is strongly presumed like the Cahuilla swarm (Ross & Cochran 2021) or the Ubaye seismic sequences (Baques *et al.* 2021), and with high-quality (precise locations and magnitudes) earthquake catalogues. For both types of swarms, we did not consider episodes with discontinuous temporal activity or with a complex geological geometry, also for the sake of simplicity.

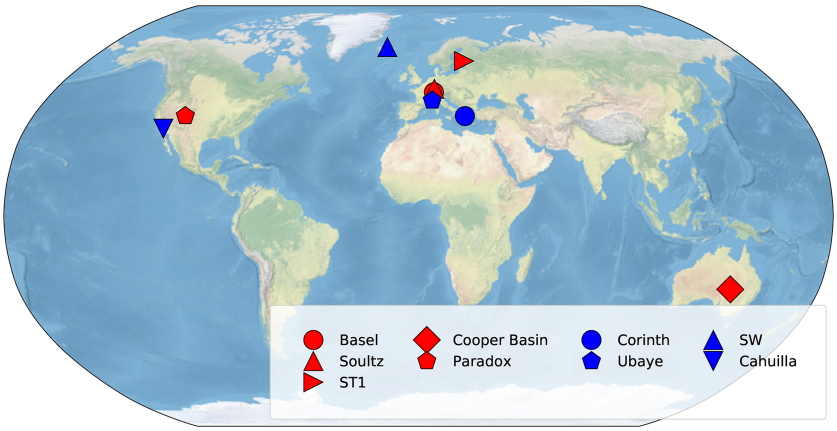

Figure 2. Map of the earthquake swarms studied here. SW corresponds to the multiple sequences studied for the swarms in Iceland (SW2; SW4, SW6; Passarelli *et al.* 2018). The Crevoux and Diemtigen swarms are not represented on the map, as they take place in the same region as the Ubaye swarm.

The injection-induced swarms studied here are for most of them associated with geothermal activities. For instance, the Basel sequence occurred in 2006 in Switzerland, following the injection of 11 500 m^3 of fluids at about 4.5 km depth over the course of ∼5 days, leading to thousands of events, including a maximum magnitude of $M_w = 3.1$ (Herrmann *et al.* 2019). The Soultz-sous-Forêt sequences happened in association with Enhanced Geothermal System (EGS) development in Eastern France, with injected fluid volumes varying from 13 000 to 37 000 m^3 at about 5 km depth, during five experimental tests between 1993 and 2003 (Gerard *et al.* 1997; Bourouis & Bernard 2007; Cuenot *et al.* 2008; Calò & Dorbath 2013). The ST1 (2018) and Cooper Basin (2003 and 2012) sequences, also induced by fluid injections for geothermal purposes, took place in Finland and Australia, with injected fluid volumes of 18 000, 20 000 and 34 000 m^3, respectively (Baisch *et al.* 2006; Baisch *et al.* 2015; Kwiatek *et al.* 2019). The Paradox Valley swarm was induced by wastewater injection at depth (4–5 km), with a tremendous amount of fluids injected (7.7 million m^3) since 1985 and several $M_w > 4$ events. More information about those sequences can be found in the Supporting Information.

The selected natural swarms occurred in diverse geological and tectonic contexts. For instance, the Corinth swarms took place in 2001 and 2015 in a rift zone with a high extensional rate, with hundreds of events for the two sequences and maximum magnitudes of 3.8 and 2.5, respectively (Duverger *et al.* 2018; De Barros *et al.* 2020). The Ubaye, Diemtigen and Crevoux swarms occurred in the French Alps (Daniel *et al.* 2011; De Barros *et al*. 2019; Simon *et al.* 2021) in 2003–2004, 2014–2015 and 2014, respectively. The first ones lasted ∼2 yr while the Crevoux swarm had only a few days of activity. The Cahuilla swarm (Ross *et al.* 2020) lasted around ∼4 yr in the vicinity of the transform fault systems of California, with the largest event culminating at $M_w = 4.4$. The Iceland swarms (SW2, SW4 and SW6) took place along a long fault system, the Husavik-Flatey fault, in 2001, 2008 and 2013 (Passarelli *et al.* 2018).

3 METHODS TO ESTIMATE FLUID VOLUME FROM INJECTION-INDUCED SEQUENCES

3.1 Method 1: total moment estimation

With the studied data sets, relating fluid volume to seismic moment is limited by the fact that existing relations are only valid when considering the aseismic contribution of the deformation in the moment estimation (De Barros *et al.* 2019). If seismicity migration (Roland & McGuire 2009; Hatch *et al.* 2020; De Barros *et al.* 2021), geodesy (Lohman & McGuire 2007; Hamiel *et al.* 2012; Gualandi *et al.* 2017), repeating earthquakes (Matsuzawa *et al.* 2004; De Barros *et al.* 2020) and effective stress drop (Fischer & Hainzl 2017) suggest the presence of aseismic slip in injection-induced sequences, its precise quantification is challenging given the depths (>5 km), durations and relatively low deformations of those episodes.

At the same time, the dynamics of aseismic fault slip has been studied through numerical modelling (Dublanchet 2019; Wynants-Morel *et al.* 2020; Yang & Dunham 2021) and field experiments (Guglielmi *et al.* 2015; Cappa *et al*. 2019). They showed that fluid injection primarily induces aseismic slip and that the shear stress perturbation resulting from its propagation triggers seismicity on rate-weakening fault asperities well oriented for dynamic rupture. Global analysis of injection-induced swarms revealed that seismicity migration in swarms can be related to an aseismic slip transient propagation (Danre *et al.* 2021; De Barros *et al.* 2021). This is similar to what happens during repeating earthquake sequences where it has been shown that the slip released seismically on asperities is driven by and equals the surrounding aseismic slip, due to the stress loading of those asperities by the aseismic transient (Matsuzawa *et al.* 2004; Uchida 2019).

Indeed, during creep events, slip released seismically by repeating earthquakes on discrete asperities embedded in a creeping medium is commonly assumed to be equal to the surrounding aseismic slip (Uchida 2019). For earthquake swarms, the low effective stress drop values found in the literature (Fischer & Hainzl 2017; Danre *et al.* 2021) suggest that seismicity may also be located on discrete asperities surrounded by aseismic regions. The aseismic slip and the resulting stress loading might then lead to the seismicity, with a seismic slip similar to the aseismic one, as shown during hydromechanical modelling (Wynants-Morel *et al.* 2020). Bourouis & Bernard 2007 also showed that the repeating events they observed during the 1993 Soultz-sous-Forêts sequence are caused by fault creep around discrete asperities, and reveal the creep rate. So, even if the density of seismic asperities might be higher in a swarm than in a creep event, seismic slip might help quantifying the aseismic slip occurring over the swarm area. Therefore, by analogy with creep studies (Uchida 2019), we then suppose that over the whole swarm area, seismic slip is occurring on discrete asperities and equals the surrounding aseismic slip, on average. We make the hypothesis that

the largest event asperity ruptures only once. We also neglect the contribution of afterslip given that it represents only ∼20 per cent of the slip occurring over the seismically slipping asperity during numerical simulations of small repeating earthquakes (Chen & Lapusta 2009). Then, pursuing the analogy with creep events triggering repeating earthquakes (Uchida 2019), the slip ($D_{\max}$) of the largest event gives an estimate of the surrounding aseismic slip occurring in between seismic asperities.

To compute $D_{\max}$ for each sequence, we suppose that the largest event has an average stress drop $\Delta\ \sigma_{\max} = \frac{7}{16}\frac{M_{0,\max}}{R_{\max}^3}$ of 10 MPa over a circular area of radius $R_{\max}$, unless a more precise value is provided in the literature (see Supporting Information). This value is representative of classical stress drop observed for global data sets of earthquakes (Gao *et al.* 2012; Cocco *et al.* 2016). Given the largest event seismic moment $M_{0,\max}$, assuming a classical value of rock shear modulus (G = 30 GPa) we estimate $D_{\max}$ with (Madariaga 1976) :

$$D_{\max} = \frac{(16\Delta\sigma_{\max})^{2/3} * (M_{0,\max})^{1/3}}{(7)^{2/3} G\pi}\ . \tag{1}$$

By analogy with fault creep sequences (Uchida 2019), we assume that the average slip over the swarm area (A) equals $D_{\max}$, allowing us to estimate the total (seismic + aseismic) moment released with :

$$M_{0,\text{total}} = G * D_{\max} * A. \tag{2}$$

To determine the swarm area A, we use a method similar to the one used in Fischer & Hainzl (2017). From the 3-D locations of hypocenters, and after removing outliers which could bias plane fitting (background seismicity or mislocated events), we determine the best-fitting plane. This can be done because hypocenters in all swarms are at first order coplanar, as revealed by the eigenvalues of their distribution (Table S1). We then project the hypocenters over this plane and remove the remaining outliers. Finally, we delineate the projected hypocenters with a convex hull to compute the swarm area A. Note that this approach cannot be used if the seismicity distribution is non-planar and should be generalized to include swarms with complex geometrical structures that are not considered here. Because of the different assumptions we make, the estimation of the aseismic component can only be considered as a rough approximation. However, this method allows us to estimate total (and therefore, including the aseismic) deformation by overcoming the limitations developed previously. Since recent studies have shown that aseismic slip can explain the discrepancy to the McGarr's law (McGarr & Barbour 2018; De Barros *et al.* 2019), its estimation should then allow to relate the injected fluid volume (V_{inj}) to the induced deformation. Assuming that aseismic slip is the only parameter responsible for the discrepancy to the McGarr's law (eq. 3a), we get :

$$M_{0,\text{seismic}} = 2 * G * V_{\text{inj}} \tag{3a}$$

$$M_{0,\text{total}} = M_{0,\text{seismic}} + M_{0,\text{aseismic}} = 2 \times G \times V_{\text{inj}}, \tag{3b}$$

where $M_{0,\text{total}}$ is the total moment released estimated with eq. (2).

Therefore, it is possible to get an estimate of the injected fluid volume by rearranging eq. (3b) as follows :

$$V_{\text{inj}} = M_{0,\text{total}}\ /\ (2 \times G)\,. \tag{4}$$

Given that we estimate total moment based on the largest event characteristics (moment and slip, eqs 1 and 2) and on the seismicity area, eq. (4) allows us to relate conventional seismic observables to the injected volume of fluids. This method is therefore fully based on the McGarr relation, but we here quantitatively consider the total moment, including its aseismic contribution. We will later validate our approach through the reconstruction of the actual injected fluid volume for injection-induced sequences.

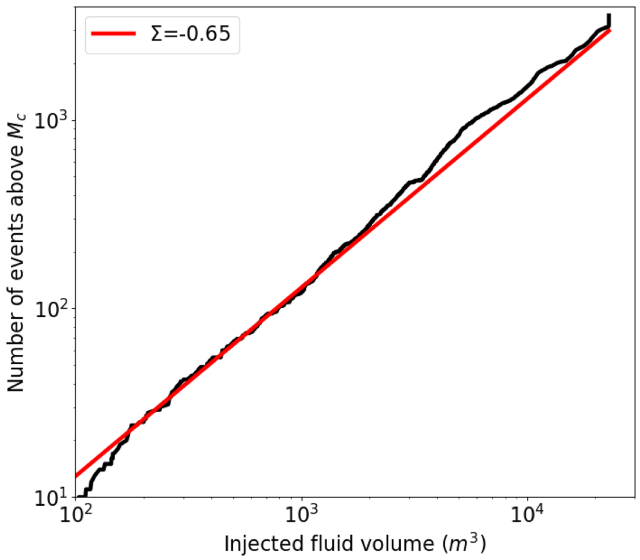

Figure 3. Number of events above completeness magnitude M_c as a function of the injected fluid volume for the Soultz 2000 sequence (black line). Red line represents the theoretical prediction assuming a seismogenic index of −0.65, following eq. (5).

3.2 Method 2: seismogenic index and effective stress drop

A second method can be developed by comparing two attributes that are commonly used to quantify the seismogenic productivity of a swarm. While the seismogenic index depends on the injected volume and is used for injection-induced swarms, the effective stress drop has also been used for natural swarms.

3.2.1 Seismogenic index and effective stress drop computation

Based on the growth of seismicity with the injected fluid volume during hydraulic injections (Fig. 3), Shapiro *et al.* (2010) introduce the seismogenic index as:

$$\Sigma\ = \log\left(N_{M_c}\right) - \log\left(V_{\text{inj}}\right) + b * M_c, \tag{5}$$

where M_c is the magnitude of completeness of the catalogue, N_{Mc} is the number of events of magnitude above M_c, b is the exponent in the Gutenberg–Richter law of the sequence and V_{inj} is the injected fluid volume.

Σ represents therefore the sensitivity of injection-induced seismicity to a fluid injection. A high value means a dominantly seismic response following an injection, while a low value means that injection only induces a sparse seismicity. Σ value is observed to be site-specific and remains constant during the injection (Shapiro *et al.* 2010). To get the value of Σ for injection-induced swarms, we use the injected volume value V_{inj} provided in the literature for each sequence. We determine the completeness magnitude M_c and the b-value of the Gutenberg–Richter law by fitting the magnitude distribution of earthquakes (see Fig. S1 and Table S2).

The effective stress drop has been used in several studies (Roland & McGuire 2009; Fischer & Hainzl 2017) to compare the seismic

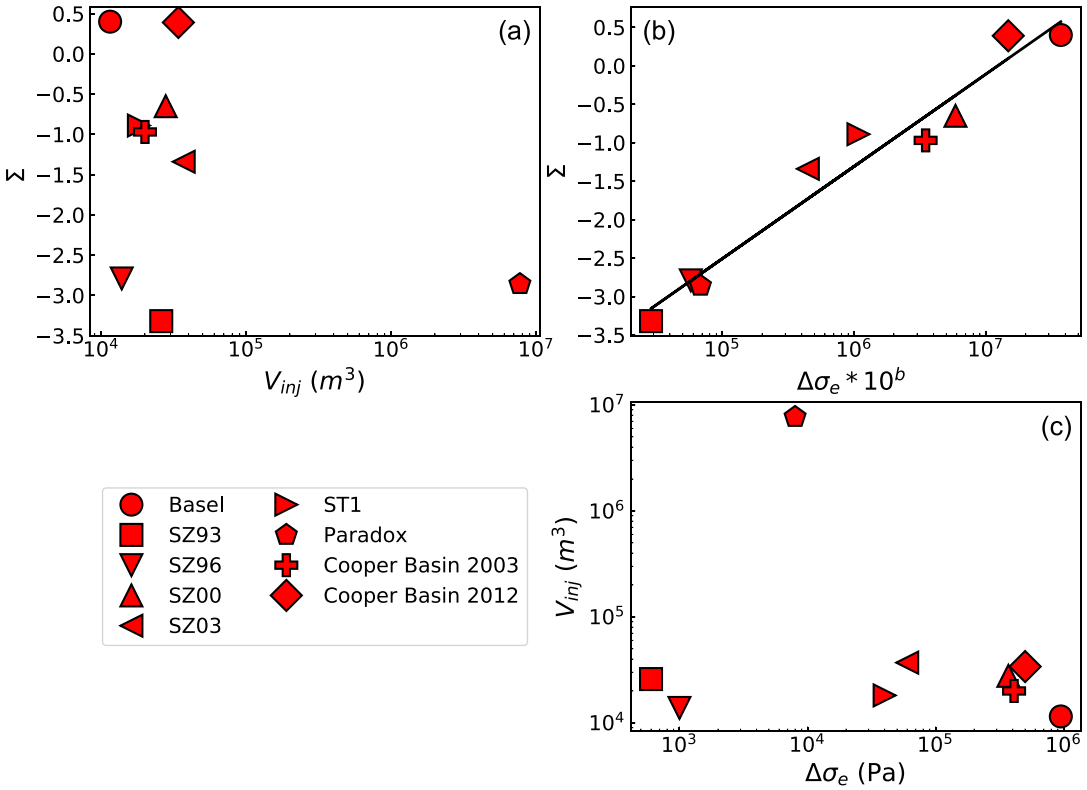

Figure 4. (a) Seismogenic index Σ (Shapiro *et al.* 2010) versus injected fluid volume V_{inj} (m^3) for the nine injection-induced sequences studied here. (b) Σ versus the product of effective stress drop $\Delta\sigma_e$ with 10^b for the same sequences. The black line represents the best linear fit. (c) Injected fluid volume V_{inj} versus $\Delta\sigma_e$.

moment released during swarms to the spatial extent of the seismicity area. By analogy with the definition of the static stress drop for a circular crack rupture (Madariaga 1976), and following Fischer & Hainzl (2017), this parameter is defined as :

$$\Delta\sigma_e = \frac{7 \times M_{0,\text{seismic}}}{16 \times R_a^3}, \tag{6}$$

where $M_{0,\text{seismic}}$ is the cumulative seismic moment released over the seismicity area and R_a the radius of this area. Similarly to Σ, low values of $\Delta\sigma_e$ indicate a sparse seismicity over the seismicity area while a high value (close to typical static stress drop values for earthquakes, for example 1–100 MPa, Cocco *et al.* 2016) corresponds to a dominantly seismic response. $\Delta\sigma_e$ has also been observed to be stable with time (Fischer & Hainzl 2017).

To get the radius R_a for the effective stress drop (eq. 6), we assume that the seismicity area A is circular, and therefore have:

$$R_a = \sqrt{\frac{A}{\pi}}. \tag{7}$$

After summation of the seismic moment of all the events within the area, we compute the effective stress drop value for the injection-induced sequences studied here.

3.2.2 Correlation between seismogenic index and effective stress drop

Both the seismogenic index and the effective stress drop are observed to describe the seismogenic behaviour of a swarm. Therefore, given the qualitative similarities between both parameters, we can compare them. Seismogenic index Σ values are widely scattered for fluid injections, despite similar volumes (Fig. 4a). Therefore, no apparent correlation is observed between Σ and V_{inj}. The same observation can be made for effective stress drop $\Delta\sigma_e$, which varies of ∼3 orders of magnitude here (Fig. 4c). The studied sequences depict a great diversity of seismogenic responses to the fluid injections, as highlighted by the large variations in Σ and $\Delta\sigma_e$ values. However, these two parameters are found to be strongly correlated (Fig. 4b). We observed that multiplying $\Delta\sigma_e$ by a factor 10^b, where the parameter b is the b-value, increases the robustness of the correlation despite the small number of data points used here (Fig. 4b, $R^2 = 0.96$). This could be because the b-value also might give information on the stress state (Scholz 2015), hence on the seismogenic state of the reservoirs. This parameter is present in the seismogenic index, but not in the effective stress drop. Without the 10^b factor, the correlation still remains robust (see Fig. S2).

The observed correlation can be written as:

$$\Sigma = p \times \log\left(\Delta\sigma_e \times 10^b\right) + q \tag{8}$$

with $p = 1.2$ and $q = -8.5$ determined by a linear fit with the nine injection-induced sequences studied here (Fig. 4b).

Based on the observed correlation (eq. 8), we can use eq. (5) to relate $\Delta\sigma_e$ to the injected fluid volume V_{inj} :

$$\log\left(V_{\text{inj}}\right) = \log(N) + b \times M_c - \left(p \times \log\left(\Delta\sigma_e \times 10^b\right) + q\right) \tag{9}$$

This leads to:

$$V_{\text{inj}} = N \times 10^{b \times (M_c - p)} \times \Delta\sigma_e^{-p} \times 10^{-q} \tag{10}$$

Therefore, based on the observed correlation between Σ and $\Delta\sigma_e$, we can relate seismic observables (number of events N, b-value,

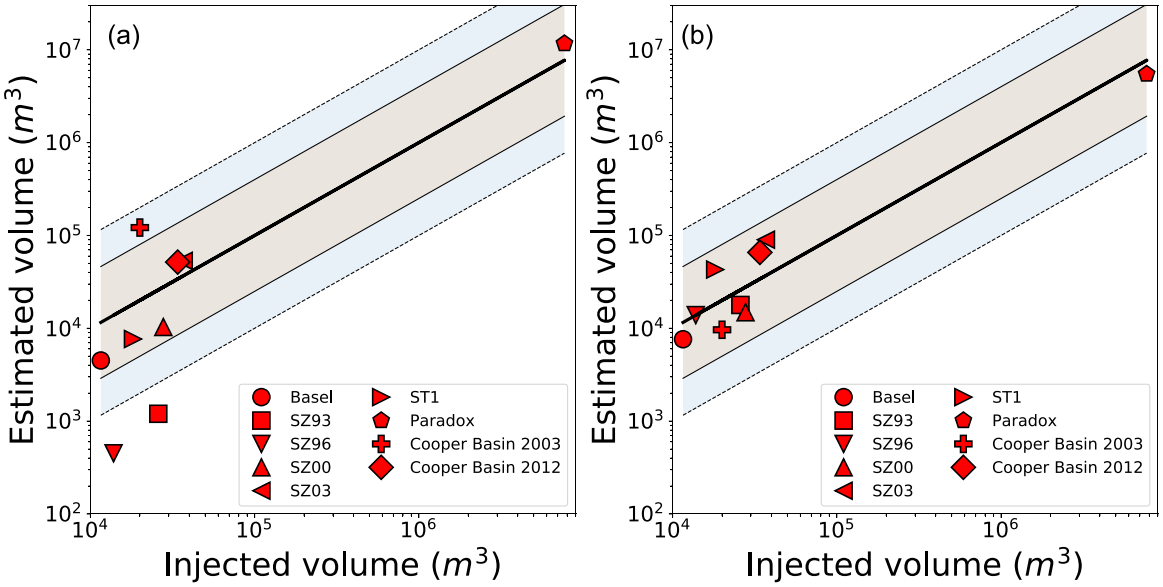

Figure 5. Comparison between estimated and measured fluid volume for the nine injection-induced sequences studied here. (a) Approach based on the total moment estimation (eq. 4). Brown-shaded area represents a factor of four difference between estimated and measured volumes while blue area represents a factor of 10. Black line represents the case of $V_{est} = V_{inj}$. (b) Same as (a) using the approach based on the seismogenic index/effective stress drop correlation (eq. 10).

effective stress drop $\Delta\sigma_e$ and empirical coefficients p and q) to the volume of fluids injected at depth. This relation between injected fluid volume and seismicity involves more parameters than the one proposed by McGarr (2014) but they remain relatively easy to compute.

4 VALIDATION OF THE FLUID VOLUME RECONSTRUCTION WITH INJECTION-INDUCED SEQUENCES

Two methods have been introduced to reconstruct the injected fluid volume. To validate the approaches, in the following, we compare the reconstructed injected volumes to the actual measured values for the injection induced sequences.

4.1 Comparison of analytical estimates with actual injected volume

Estimating fluid volume based on the total moment computation (Method 1, eq. 4) leads to scattered results around the best theoretical line (Fig. 5a, black line). Except the Cooper Basin 2003, Soultz 1993 and 1996 cases, the volume is reasonably well reconstructed within an acceptable range, as all volumes can be estimated with at most a factor 4 difference (Fig. 5a) compared to the measured injected volume. This gives a degree of confidence that our approach is sound. This agreement therefore validates our total moment estimations for most of the cases, as well as our assumption that the discrepancy with the McGarr's law is only due to aseismic slip and our analogy with repeating events in creeping cases.

However, the volume is slightly overestimated for the Cooper Basin 2003 sequence, and it is strongly underestimated by ∼2 orders of magnitude for the Soultz 1993 and 1996 cases. Important aseismic release can be expected for those two Soultz sequences as their cumulative seismic moment is already 2–3 orders of magnitude smaller than the seismic moments of the other injections despite similar injected volumes (see Figs 1b and c). These two injections also exhibit much lower effective stress drop and seismogenic indices than the other cases (Fig. 3). Therefore, aseismic slip seems to be strongly underestimated in our total moment computation. This may come from one of the strong hypotheses made, like considering that the maximum seismic slip of the largest event equals the average aseismic slip.

The method based on the seismogenic index/effective stress drop correlation (Method 2, eq. 10) leads to more constrained estimates of the injected fluid volume, when comparing it to its actual value (Fig. 5b). Indeed, estimated values are all within a factor 4 range of the true value of the injected fluid volume. The discrepancies could be explained by uncertainty in the effective stress drop calculation, especially with the plane fitting and area computation. This parameter computation is indeed based on a strong assumption that all events are located on a single plane, which seems to be realistic at first order for the studied sequences (Table S2). Despite all this, the use of this method still allows to get a quite precise estimate of the fluid volume injected, based only on the computation of common seismic parameters.

Contrary to the previous approach based on total moment estimate, the use of the empirical correlation between Σ and $\Delta\sigma_e$ does not require to make hypothesis on the aseismic slip value, which might explain why the volume estimates of Soultz 1993 and 1996 sequences are more consistent (Figs 5a and b). The accurate reconstruction of the fluid volume shows that additional parameters have to be considered to include aseismic component in the seismicity–volume relations.

4.2 Effective stress drop and seismogenic index depict slip partitioning

The use of the correlation between Σ and $\Delta\sigma_e$ gives better estimates but remains empirical. We show below that this correlation can be explained by aseismic moment release over the seismicity area. It

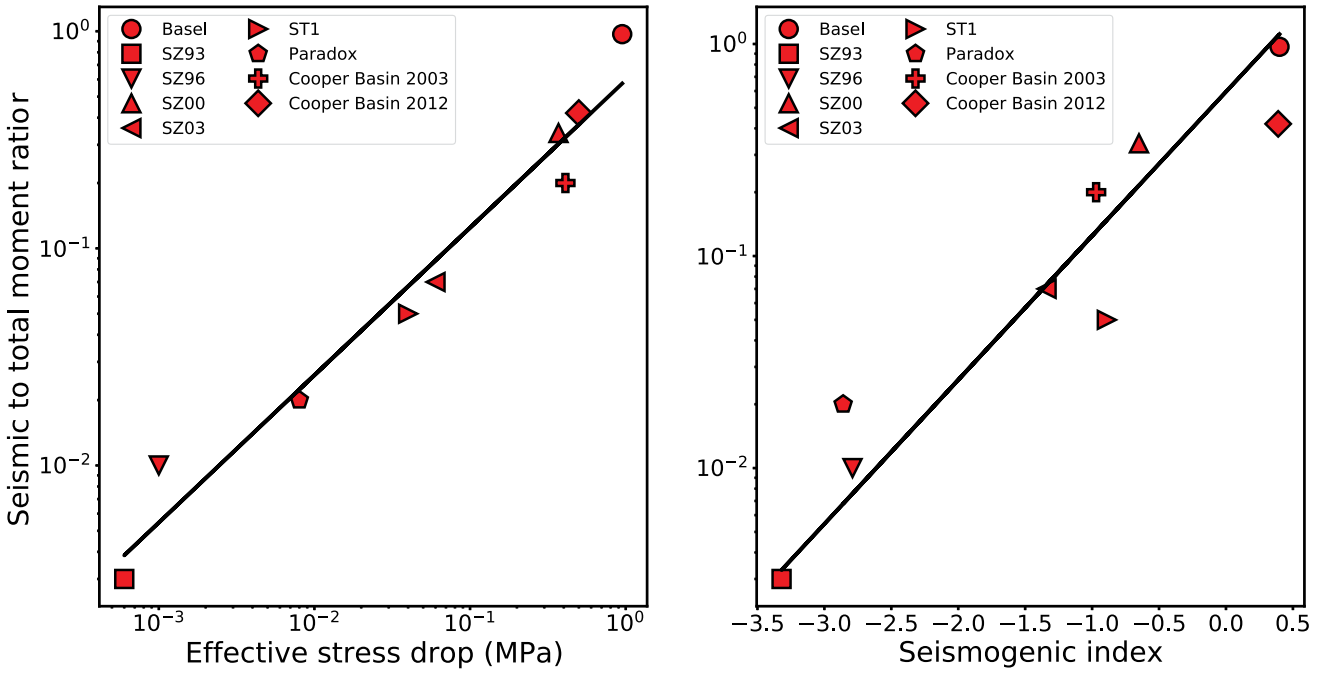

Figure 6. (a) Estimated seismic to total moment ratio r as a function of effective stress drop, for the nine injection-induced earthquake swarms studied here. Black line represents the best fit ($R^2 = 0.96$). (b) Same but with seismic to total moment ratio as a function of the seismogenic index. In this case, $R^2 = 0.90$.

leads to a new interpretation of the seismogenic index, similar to the one of the effective stress drop.

Indeed, let us assume that aseismic slip occurs over the seismicity area, supposed to be circular. Then, one can define the total (seismic + aseismic) stress drop of the slip event :

$$\Delta\sigma_{\text{total}} = \frac{7 * M_{0,\text{total}}}{16 * R^3} \tag{11}$$

where the total moment $M_{0,\text{total}} = M_{0,\text{seismic}} + M_{0,\text{aseismic}}$ takes into account the aseismic moment released. So, from eqs (6) and (11), we get :

$$\log(\Delta\sigma_e) = \log\left(\frac{M_{0,\text{seismic}}}{M_{0,\text{total}}}\right) + \log\left(\Delta\sigma_{\text{total}}\right) \tag{12}$$

Because $M_{0,\text{seismic}} < M_{0,\text{total}}$, the logarithm is negative and so the effective stress drop is smaller than the total stress drop. Therefore, effective stress drop can then be seen as a function of the seismic to total moment ratio $r = \frac{M_{0,\text{seismic}}}{M_{0,\text{total}}}$ and of the total stress drop. The lower r is, the lower the effective stress drop, as depicted on Fig. 6(a).

Assuming that seismicity follows a Gutenberg–Richter law with the b-value (b) and $M_{\text{w,max}}$ the maximum magnitude, the seismogenic index can be written (Van der Elst *et al.* 2016) as :

$$\Sigma = b \times M_{\text{w, max}} - \log\left(V_{\text{inj}}\right) \tag{13}$$

If we suppose that McGarr (2014) law applies to the total moment released, as seems to be validated by results from method 1 (Fig. 5a), then using eq. (4), we get:

$$\Sigma = b \times M_{\text{w, max}} - \log\left(\frac{M_{0,\text{total}}}{2 \times G}\right) \tag{14}$$

Then we get :

$$\Sigma = \frac{2b}{3} \times \log(M_{0,\text{max}}) - 6.07 \times b - \log\left(M_{0,\text{total}}\right) + \log\left(2 \times G\right) \tag{15}$$

where $M_{0,\text{max}}$ is the maximum moment. Finally, assuming that $b = 1.5$ for simplicity purposes here :

$$\Sigma = \log\left(\frac{M_{0,\text{max}}}{M_{0,\text{total}}}\right) + \log\left(2 \times G\right) - 6.07 \times b \tag{16}$$

As $M_{0,\text{max}}$ is related to the cumulative seismic moment $M_{0,\text{seismic}}$ (Wyss 1973), Σ is also depending on the seismic-to-total ratio, like Fig. 6(b) shows. It might therefore reflect a partitioning between seismic and aseismic slip.

Following the expression found for the effective stress drop (eq. 12) and the seismogenic index (eq. 16) we can see that both parameters are function of a ratio involving the released seismic moment divided by total moment.(Figs 6a and b). They can therefore be interpreted in a similar way, as depicting the partitioning between seismic and aseismic slip.

5 APPLICATION TO NATURAL EARTHQUAKE SWARMS

Based on injection-induced catalogues, we validated the two methods to reconstruct the injected fluid volume only using seismological observables. We can then estimate the volume of fluids circulating during natural swarms based solely on earthquake catalogues.

5.1 Estimation of the fluid volume for natural swarms

Assuming that natural swarms are caused by the same mechanisms as injection-induced sequences (Danré *et al.* 2021), we can therefore apply eqs (4) and (10) to those sequences, to infer the volume of circulating fluids. After computing the seismic observables (completeness magnitude, b-value, number of events, effective stress drop), we can reconstruct fluid volume values for the nine natural swarms studied here, with the two methods developed previously. Using the

Table 1. Fluid volume estimates, taken as an average of results from Methods 1 and 2 (except *) for the natural swarms studied here, along with the parameters used in eq. (10). Estimated total moment ($M_{0,\text{total}}$), obtained from eqs (1) and (2) is also given. * : estimated only using the correlation between seismogenic index and effective stress drop (Method 2).

Name of seismic swarms	$N_{\geq M_c}$	b	M_c	$M_{0,\text{seismic}}$ (N.m)	$\Delta\sigma_e$ (MPa)	Estimated Σ	Estimated $M_{0,\text{total}}$ (N.m)	V_{est} (m^3)	Average flowrate ($L\,s^{-1}$)
Corinth 2001	1641	1.12	1.1	3.2E + 15	0.083	−1.3	4.7E + 16	6.4E + 5	21
Corinth 2015	867	1.6	0.9	1.4E + 14	0.97	0.6	2.6E + 14	5.1E + 3	12
Cahuilla	8963	1.44	1.2	1.0E + 16	0.22	−0.4	8.6E + 16	1.3E + 6	14
SW2	576	0.93	0.6	4.0E + 14	0.046	−1.8	8.5E + 15	1.4E + 5	78
SW4	210	1.7	1.6	3.6E + 14	0.0027	−2.3	3.9E + 16	2.5E + 7*	2.2E + 4*
SW6	717	0.93	1.1	2.2E + 15	0.02	−2.2	1.0E + 17	1.5E + 6	1.5E + 3
Crevoux	216	0.75	−0.4	9.4E + 12	0.2	−1.2	7.0E + 13	1.5E + 3	2.8
Ubaye	709	1.0	0.6	1.7E + 14	0.001	−3.7	3.4E + 16	1.4E + 7*	253*
Diemtigen	353	1.08	0.6	1.2E + 14	1.04	0.0	3.77E + 14	3.9E + 3	0.14

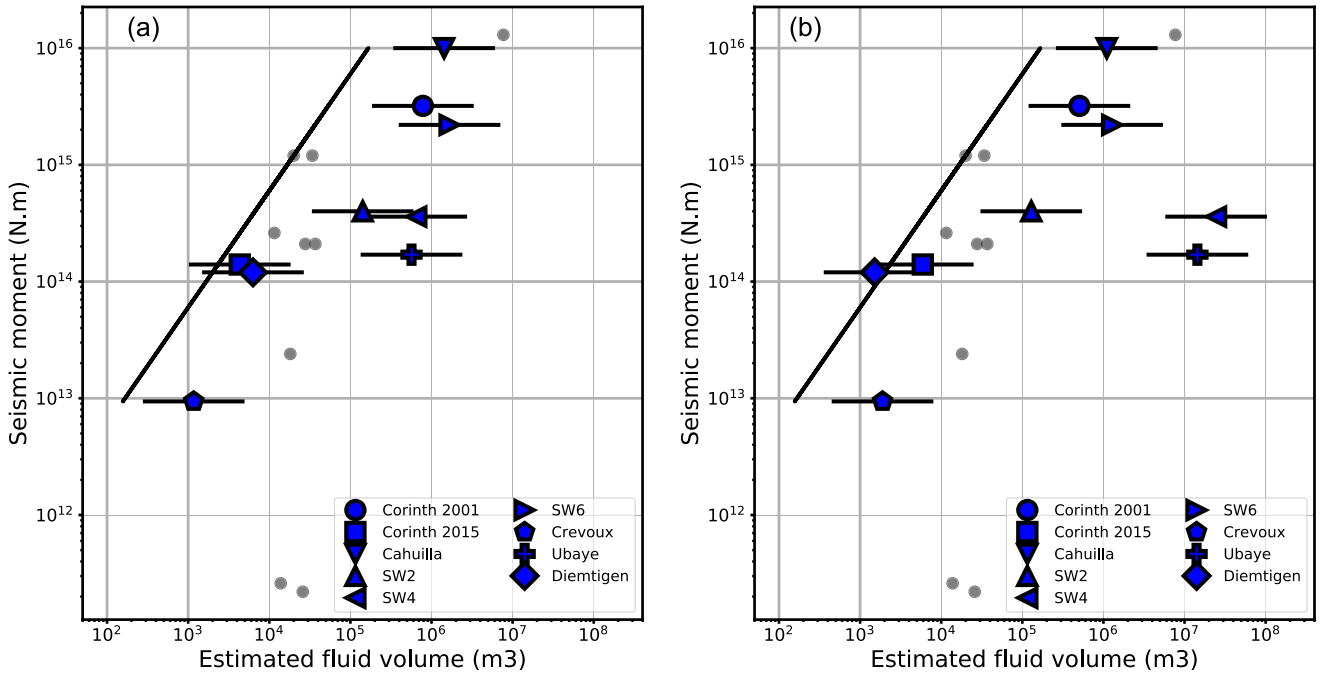

Figure 7. Fluid volumes estimated for natural swarms using (a) the computation of total moment (eq. 4) and (b) the correlation seismogenic index/effective stress drop (eq. 10). Here, we represent the cumulative seismic moment as a function of the estimated fluid volume. Black line represents $M_{0,\text{seismic}} = 2 \times G \times V_{\text{fluids}}$ (McGarr & Barbour 2018) while horizontal bars represent the estimated uncertainties (factor of 4 difference). For comparison, actual seismic moment and the measured injected volume for injection-induced sequences is shown (grey dots)

correlation between seismogenic index and effective stress drop, we use the same values of p and q as determined for injection-induced sequences (eq. 8). Based on the observations made in Fig. 5, we consider a factor 4 error in our volume estimate for both methods.

The estimated fluid volume values are summarized in Table 1 and shown in Fig. 7. Apart from Ubaye and SW4, volumes found with the two methods are similar, within the factor 4 uncertainty range (Figs 7a and b). It gives confidence in the reliability of the estimations, as the two approaches do not rely on the same hypotheses (aseismic estimation for the first one, and empirical correlation between Σ and $\Delta\sigma_e$ for the second). In this case, we take as final volume value the mean between the two estimates. For instance, during the 4 years long swarm of Cahuilla (Ross *et al.* 2020), the circulating fluid volume would be of around 1.3×10^6 m^3. In the Corinth case, the volume of fluids circulating during the 2015 swarm (De Barros *et al.* 2020) would be of around 5100 m^3. Interestingly, this swarm presents many similarities with the 2006 Basel sequence in terms of duration, propagation of seismicity and magnitude (Danré *et al.* 2021). Finding for Corinth a volume estimate similar to the injected volume in Basel (11 500 m^3) highlights this similarity.

For the Ubaye and SW4 swarms, estimates from the two approaches differ by 1.5 orders of magnitude. Those two sequences exhibit low effective stress drops compared to the other natural swarms (Table 1), but the same order of magnitude as the ones of the Soultz 1993 and 1996 sequences. We observed previously that the method based on total moment computation does not reconstruct reliably the injected fluid volume for the two Soultz sequences because the contribution of aseismic slip was strongly underestimated. Therefore, as suggested by the low effective stress drop values, we can suppose that total moment underestimation explains the discrepancy between the two estimates for SW4 and Ubaye. For these two cases, we keep only the volume estimate based on

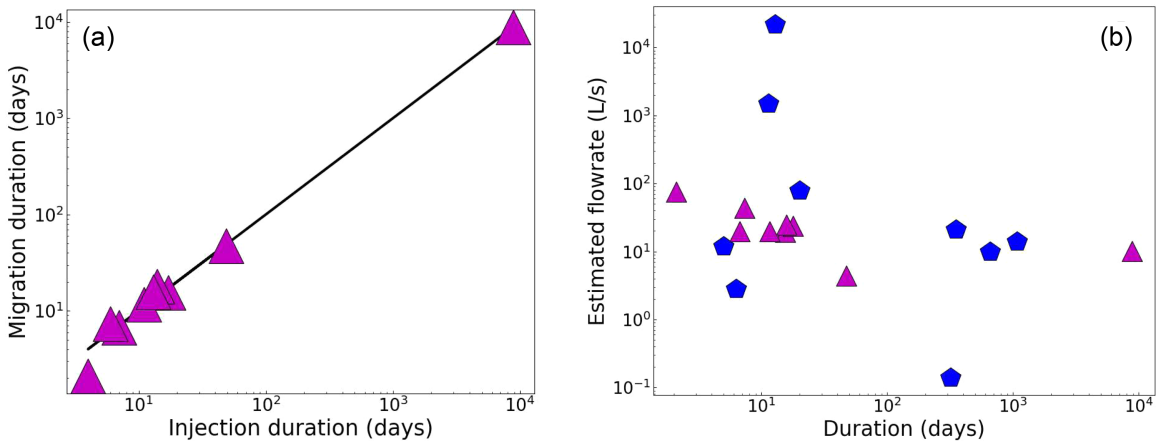

Figure 8. (a) Migration duration versus injection duration, in days, for the nine studied injection-induced swarms. Black lines represent the 1:1 scaling. (b) Estimated average flowrate for natural swarms (blue pentagons) and injection-induced sequences (magenta triangles), in L s^{-1}. Flowrate is computed following eq. (17) in both cases.

the correlation between effective stress drop and seismogenic index (Method 2).

By applying eqs (4) and (10), validated with injection-induced sequences, to natural swarms, we are able to estimate the volume of fluids circulating at depth during natural earthquake swarms, only using seismic observables requiring typical earthquake catalogues (magnitudes, locations). Moreover, as both approaches rely on different assumptions, comparing their respective results allow us to validate the reliability of the results.

5.2 Similarities with injection-induced seismicity

First, the effective stress drops and the estimated seismic-to-total ratio falls within the same range for natural and injection-induced seismic swarms. Effective stress drops are indeed found between ∼1 kPa and ∼1 MPa in both cases (Danré *et al.* 2021). Moreover, the estimation of the volume allows the computation of the seismogenic indexes for natural swarms (Table 1). They show similar values of Σ with injection-induced sequence ones, underlining the similarities between the natural and injection-induced sequences.

Migration duration for swarms is determined empirically as the time during which the distance of the seismicity front to the first few earthquakes increases (Danré *et al.* 2021). For injection-induced sequences, migration duration is nearly identical to the injection duration (Fig. 8a), as the fluid injection is the primary mechanism triggering and maintaining slip (seismic or aseismic) with time. Therefore, we assume that migration duration for natural swarms indicates the duration of the fluid pressure perturbation.

For the Corinth 2015 swarm, injection duration is then ∼5 d, while for Cahuilla, injection lasts around 1000 d.

We can then estimate an apparent fluid flowrate (Q) using :

$$Q = \frac{V_{\text{est}}}{T}, \tag{17}$$

where V_{est} is the estimated fluid volume (m^3) and T is the migration duration.

Values of Q for natural swarms range between 0.14 and 22 000 L s^{-1}, with all but three of them (Ubaye, SW4 and SW6) between 2.8 and 57 L s^{-1} (Table 1). Those values are similar to typical values for the injections studied here (Fig. 8b): for Basel, flow reaches 50 L s^{-1} (Goertz-Allman *et al.* 2011) while for Cooper Basin it is up to 40 L s^{-1} (Baisch *et al.* 2006) for instance. Our results are also in accordance to other attempts made to estimate fluid volume and flowrate during earthquake swarms like in Bachura *et al.* 2021 where during an earthquake swarm in Western Bohemia, estimated volumes and flowrates were of 6400 m^3 and ∼30 L s^{-1}, respectively. The particularly high value of Q for SW4 and SW6 could be due to a singular mechanism of fluid circulation for those sequences, or to an overestimation of the circulating fluid volume. In addition to finding similar volumes for similar swarms, we therefore show that swarms seem triggered by fluid injections with flow of similar orders of magnitude, despite different durations or estimated volumes.

6 DISCUSSION ON THE PROPOSED METHODS

6.1 Relating operational injection parameters to seismic observables

The interest in using the two previous methods to relate fluid volume to the observed seismicity can be seen when comparing them to other methods existing in the literature. As already stated, using directly $M_{0,\text{seismic}} = 2 \times G \times V_{\text{inj}}$ (McGarr 2014) leads to major differences in the expected versus actual cumulative seismic moment when considering a shear modulus G value of 30 GPa (Fig. 1b) because of the aseismic slip release occurring at the same time (McGarr & Barbour 2018; De Barros *et al.* 2019). Similarly, Galis *et al.* (2017) do not consider aseismic contributions in their physics-based framework that relates maximum seismic moment with injected fluid volume.

To consider the aseismic contribution, Van der Elst *et al.* (2016) used the seismogenic index in order to link the observed maximum seismic moment to the injected fluid volume. Therefore, such a framework cannot be used if the aim is to reconstruct the volume, given that the seismogenic index computation requires to know the volume of fluids circulating (eq. 5).

Therefore, the framework developed in this study, to relate seismicity with fluid volume, is of particular interest as: (1) it is only based on seismological data and only requires a detailed catalogue of seismicity; (2) it relies on crude but simple assumptions and fast computations like a Gutenberg–Richter law fitting and (3) it does

not require the precise knowledge of physical parameters like fault friction coefficients and other hydromechanical properties. The two methods developed here use different and independent assumptions : the first is based on physical concepts, but it relies on many hypotheses, while the second is based on an empirical observation and leads to more accurate volume estimation. Despite that, in most of the cases, they lead to consistent results, validating each other. Also, Method 1 shows the importance of taking into account aseismic and therefore total moment release to explain the observations on which Method 2 is based. It therefore provides a good degree of confidence in our approaches which are well adapted whatever the tectonic setting hosting the swarm. Finally, a side-product of our approach is the computation of the seismic-to-aseismic ratio for both natural and injection-induced swarms. However, such estimation has to be taken with caution, as the used assumptions seems to fail for the most aseismic sequences ($\Delta\sigma_e$ lower than $\sim$10 kPa).

The invariance in time of both Σ and $\Delta\sigma_e$, which are both related to the seismic to total moment ratio, suggests that such a ratio should not vary during swarms, and therefore is controlled by structural parameters (i.e. frictional properties, stress-state, criticality of the faults, asperity distribution and size). Assessment of this ratio, so of the aseismic moment released, is of great importance for (1) anthropic injections as it depicts the evolution of seismicity with the injected volume and (2) natural swarms and hazard assessment as it gives information about the rupture process taking place.

As our approach only depends on seismic catalogues, it might also depend on the catalogue quality. Particularly, the magnitude estimation should be crucial for effective stress drop and total moment estimate, but magnitudes are often determined with a 0.2-to-0.5 error (e.g. Daniel 2014). In the data set of injection-induced cases we used to calibrate the methods, catalogues are of different quality: some of them are relocated (e.g. Basel) and some are not (e.g. Soultz 1993), with recording networks of different qualities. However, the largest events are the ones having the most importance in the two methods developed here, and their magnitude are often determined with the more accuracy as they are usually validated with regional networks (Herrmann *et al*. 2019; Baisch *et al.* 2015). b value determination is also performed with an uncertainty $<$0.2 units which might add uncertainty in the computation of the estimated volume following Method 2 (Table S2).

However, despite the differences in quality and uncertainties, both methods allow us to reconstruct fluid volume with a very acceptable precision for injection-induced sequences, which serves as a validation. This precision could be improved with a systematic computation of magnitude uncertainty in earthquake swarm catalogues, or, in the case of the total moment estimate, with the computation of the main event stress drop. Nevertheless, those methods seem robust enough even with catalogues of various quality.

6.2 Application of our results to other types of swarms

Our observations for injection-induced sequences were based on seismicity triggered by single injections mostly during geothermal activities or wastewater disposal. Dinske & Shapiro (2013) computed seismogenic indexes for seismicity triggered by injection in shales and associated to gas production. Values are lower (Σ < -4) than for other types of injections (Σ > -4). Fischer & Hainzl (2017) also computed effective stress drop values for similar sequences, and found values of $\Delta\sigma_e \sim 1$ kPa. Therefore, despite the fact that we did not analyse them in our present work, our results might also apply to injections in shale formations, associated with gas production, as in those cases both Σ and $\Delta\sigma_e$ have low values.

In our work, we considered only swarms with a simple geometry, mainly because of the assumptions made to compute the effective stress drop. However, more complex sequences exist (e.g. Shelly *et al.* 2013). If the hypocentres were distributed volumetrically, the radius would be underestimated, which then would lead to an overestimation of the effective stress drop, following eq. (6). Estimating effective stress drop for complex geometry requires either to decompose the fault networks into individual faults or to generalize its definition by considering a correction factor based on the geometry. We also did not consider swarms occurring in volcanic context. In this particular case, relations between moment and volume exist and seem reliable (White & McCausland 2016) but the processes taking place might not be the same, as the high temperature may change the way that aseismic deformation develops. We also did not study swarms taking place in subduction zones.

Some swarms were also shown to be driven solely by slow-slip, either in crustal areas (Lohman & McGuire 2007) or along subduction interfaces (Passarelli *et al.* 2021). Therefore, the approaches developed here are meaningless for such sequences. A proper way to discriminate between fluid-driven or slow-slip driven swarms, if possible, is therefore required. One possibility for that lies in the migration velocities, as fluid-induced sequences show lower migration velocities than slow-slip triggered swarms, even if it depends on the swarm duration (Danré *et al.* 2021).

Finally, we here voluntary exclude from our analysis the injection cases where induced seismicity is shown to be above the theoretical limit defined by the McGarr's law (McGarr 2014) like the 2017 Pohang (Bentz *et al.* 2020) or the St Gallen (Diehl *et al.* 2017) sequences. In these specific cases, the injection has triggered large earthquakes whose energy is much larger than the one brought by the injection, which may be explained by the fact that activated faults were in a very critical stress state toward failure. These cases are however of great interest for risk mitigation. Therefore, a particular attention should be used when using the proposed relations, and this work should be extended to account for these particular cases.

7 CONCLUSIONS

In this work, we analysed nine injection-induced earthquake sequences to calibrate two new relations between conventional seismic observables and the injected fluid volume. Those two relations highlight the importance of taking into account aseismic slip release in the energy budget of fluid induced swarms. As they give reliable estimates of the injected fluid volume for the injection-induced swarms, we make profit of those relations to compute the initially unknown volume circulating during natural earthquake swarms. In addition to the observed similarities already studied, like seismicity migration, we find consistent orders of magnitude of fluid volume and flowrate for natural earthquake swarms. As the fluid volume acting in swarms is a key parameter difficult to measure in a natural fault system, our study paves a new way towards a precise understanding of the processes occurring at depth during those sequences, and further work may help constrain the temporal dynamics controlling natural earthquake swarms.

DATA AVAILABILITY

Data for the Iceland swarms were kindly made available by the Icelandic Meteorological Office (SIL, https://en.vedur.is/) and

L. Passarelli (Passarelli *et al.* 2018). Data from the Ubaye swarm and from the 2001 Corinth swarm were made available by G. Daniel (Daniel *et al.* 2011) and H. Lyon-Caen (Duverger *et al.* 2018), respectively. Catalogue for the Cahuilla swarm were provided by Z. Ross and D. Trugman (Ross *et al.* 2020). Data for the Soultz-sous-Forêts fluid injections were kindly provided by GEIE Exploitation Minière de la Chaleur and distributed on the CDGP web services (https://cdgp.u-strasbg.fr/, EOST & GEIE EMC 2017, GEIE EMC & EOST 2019, GEIE EMC & EOST 2018, EOST & GEIE EMC 2018). Data for the Cooper Basin injections are available on the EPOS platform (https://tcs.ah-epos.eu/). Data for the Paradox Valley fluid injection are available on the U.S. Bureau of Reclamation (https://www.usbr.gov/uc/progact/paradox/index.html). Additional references for the catalogues used can be found in the Supporting information (Text S1 and Table S3). We thank the editor A. Barbour, T. Fisher and an anonymous reviewer for their helpful comments.

CONFLICT OF INTEREST

The authors declare that they have no known competing financial interests or personal relationships that could have appeared to influence the work reported in this paper

REFERENCES

Bachura, M., Fischer, T., Doubravová, J. & Horálek, J., 2021. From earthquake swarm to a main shock aftershocks: the 2018 activity in west Bohemia/Vogtland, *Geophys. J. Int.,* **224**(3), 1835–1848.

Baisch, S., Rothert, E., Stang, H., Vörös, R., Koch, C. & McMahon, A., 2015 Continued geothermal reservoir stimulation experiments in the Cooper Basin (Australia), *Bull. seism. Soc. Am.,* **105**(1), 198–209

Baisch, S., Weidler, R., Vörös, R., Wyborn, D. & de Graaf, L., 2006. Induced seismicity during the stimulation of a geothermal HFR reservoir in the Cooper Basin, Australia, *Bull. seism. Soc. Am.,* **96**(6), 2242–2256.

Baques, M., De Barros, L., Duverger, C., Jomard, H., Godano, M., Courboulex, F. & Larroque, C., 2021. Seismic activity in the Ubaye Region (French Alps): a specific behaviour highlighted by mainshocks and swarm sequences, *Comp. Rend. Géosci.,* **353**(S1), 1–25.

Bentz, S., Kwiatek, G., Martínez-Garzón, P., Bohnhoff, M. & Dresen, G., 2020. Seismic moment evolution during hydraulic stimulations, *Geophys. Res. Lett.,* **47**(5), doi:10.1029/2019GL086185.

Bourouis, S. & Bernard, P., 2007. Evidence for coupled seismic and aseismic fault slip during water injection in the geothermal site of Soultz (France), and implications for seismogenic transients, *Geophys. J. Int.,* **169**(2), 723–732.

Calò, M. & Dorbath, C., 2013. Different behaviours of the seismic velocity field at Soultz-sous-Forêts revealed by 4-D seismic tomography: case study of GPK3 and GPK2 injection tests, *Geophys. J. Int.,* **194**(2), 1119–1137.

Cappa, F., Scuderi, M. M., Collettini, C., Guglielmi, Y. & Avouac, J.-P., 2019. Stabilization of fault slip by fluid injection in thelaboratory and in situ, *Sci. Adv.,* **5**(3), eaau4065, doi:10.1126/sciadv.aau4065.

Chen, T. & Lapusta, N., 2009. Scaling of small repeating earthquakes explained by interaction of seismic and aseismic slip in a rate and state fault model, *J. geophys. Res.,* **114**(B1), doi:10.1029/2008JB005749.

Chen, X., Shearer, P. M. & Abercrombie, R. E., 2012. Spatial migration of earthquakes within seismic clusters in Southern California: evidence for fluid diffusion, *J. geophys. Res.,* **117**(B4), doi:10.1029/2011JB008973.

Cocco, M., Tinti, E. & Cirella, A., 2016. On the scale dependence of earthquake stress drop, *J. Seismol.,* **20**(4), 1151–1170.

Cuenot, N., Dorbath, C. & Dorbath, L., 2008. Analysis of the microseismicity induced by fluid injections at the EGS site of Soultz-sous-Forêts (Alsace, France): implications for the characterization of the geothermal reservoir properties, *Pure appl. Geophys.,* **165**(5), 797–828.

Daniel, G., 2014. Bias in magnitude for earthquakes with unknown focal mechanism, *Geophys. Prospect.,* **62**(4), 848–861.

Daniel, G., Prono, E., Renard, F., Thouvenot, F., Hainzl, S., Marsan, D. & Guiguet, R., 2011. Changes in effective stress during the 2003–2004 Ubaye seismic swarm, France, *J. geophys. Res.,***116**(B1), doi:10.1029/2010JB007551.

Danré, P., De Barros, L., Cappa, F. & Ampuero, J. P., 2021. Fluid-induced anthropogenic and natural earthquake swarms are both driven by aseismic slip, *Earth and Space Science Open Archive,* 19, doi:10.1002/essoar.10509508.1.

De Barros, L., Baques, M., Godano, M., Helmstetter, A., Deschamps, A., Larroque, C. & Courboulex, F., 2019. Fluid-induced swarms and coseismic stress transfer: a dual process highlighted in the aftershock sequence of the 7 April 2014 earthquake (Ml 4.8, Ubaye, France), *J. geophys. Res.,* **124**(4), 3918–3932.

De Barros, L., Cappa, F., Deschamps, A. & Dublanchet, P., 2020. Imbricated aseismic slip and fluid diffusion drive a seismic swarm in the Corinth Gulf, Greece, *Geophys. Res. Lett.,* **47**(9), doi:10.1029/2020GL087142.

De Barros, L., Cappa, F., Guglielmi, Y., Duboeuf, L. & Grasso, J. R., 2019. Energy of injection-induced seismicity predicted from in-situ experiments, *Sci. Rep.,* **9**(1), 1–11.

De Barros, L., Wynants-Morel, N., Cappa, F. & Danré, P., 2021. Migration of fluid-induced seismicity reveals the seismogenic state of faults, *J. geophys. Res.,* **126**(11), doi:10.1029/2021JB022767.

Di Luccio, F., Ventura, G., Di Giovambattista, R., Piscini, A. & Cinti, F. R., 2010. Normal faults and thrusts reactivated by deep fluids: the 6 April 2009 Mw 6.3 L'Aquila earthquake, central Italy, *J. geophys. Res.,* **115**(B6), doi:10.1029/2009JB007190, 20.

Diehl, T., Kraft, T., Kissling, E. & Wiemer, S., 2017. The induced earthquake sequence related to the St. Gallen deep geothermal project (Switzerland): fault reactivation and fluid interactions imaged by microseismicity, *J. geophys. Res.,* **122**(9), 7272–7290.

Dinske, C. & Shapiro, S. A., 2013. Seismotectonic state of reservoirs inferred from magnitude distributions of fluid-induced seismicity, *J. Seismol.,* **17**(1), 13–25.

Dublanchet, P., 2019. Fluid driven shear cracks on a strengthening rate-and-state frictional fault, *J. Mech. Phys. Solids,* **132,** doi:10.1016/j.jmps.2019.07.015.

Duboeuf, L., De Barros, L., Cappa, F., Guglielmi, Y., Deschamps, A. & Seguy, S., 2017. Aseismic motions drive a sparse seismicity during fluid injections into a fractured zone in a carbonate reservoir, *J. geophys. Res.,* **122**(10), 8285–8304.

Duverger, C., Lambotte, S., Bernard, P., Lyon-Caen, H., Deschamps, A. & Nercessian, A., 2018. Dynamics of microseismicity and its relationship with the active structures in the western Corinth Rift (Greece), *Geophys. J. Int.,* **215**(1), 196–221.

Eaton, D. W. & Schultz, R., 2018. Increased likelihood of induced seismicity in highly overpressured shale formations, *Geophys. J. Int.,* **214**(1), 751–757.

Ellsworth, W. L., 2013. Injection-induced earthquakes, *Science,* **341**(6142), doi:10.1126/science.1225942.

EOST & GEIE EMC, 2017. Episode: 1993 stimulation Soultz-sous-Forêts [Collection]. EOST - CDGP.

EOST & GEIE EMC, 2018. Episode: 2003 stimulation Soultz-sous-Forêts [Collection], EOST - CDGP.

Eyre, T. S., Eaton, D. W., Garagash, D. I., Zecevic, M., Venieri, M., Weir, R. & Lawton, D. C., 2019. The role of aseismic slip in hydraulic fracturing–induced seismicity, *Sci. Adv.,* **5**(8), doi:10.1126/sciadv.aav7172.

Eyre, T. S., Samsonov, S., Feng, W., Kao, H. & Eaton, D. W., 2022. InSAR data reveal that the largest hydraulic fracturing-induced earthquake in Canada, to date, is a slow-slip event, *Sci. Rep.,* **12**(1), 1–12.

Fischer, T. & Hainzl, S., 2017. Effective stress drop of earthquake clusters, *Bull. seism. Soc. Am.,* **107**(5), 2247–2257.

Fischer, T. & Hainzl, S., 2021. The growth of earthquake clusters, *Front. Earth Sci.,* **9,** 79.

Fischer, T., Horálek, J., Hrubcová, P., Vavryčuk, V., Bräuer, K. & Kämpf, H., 2014. Intra-continental earthquake swarms in West-Bohemia and Vogtland: a review, *Tectonophysics,* **611,** 1–27.

Galis, M., Ampuero, J. P., Mai, P. M. & Cappa, F., 2017. Induced seismicity provides insight into why earthquake ruptures stop, *Sci. Adv.,* **3**(12), eaap7528.

Gao, H., Schmidt, D. A. & Weldon, R. J., 2012. Scaling relationships of source parameters for slow slip events, *Bull. seism. Soc. Am.,* **102**(1), 352–360.

GEIE EMC & EOST, 2018. *Episode: 2000 stimulation Soultz-sous-Forêts* [Collection], EOST - CDGP.

GEIE EMC & EOST, 2019. *Episode: 1996 Stimulation and Hydraulic Tests Soultz-sous-Forêts,* EOST-CDGP.

Gerard, A., Baumgärtner, J., Baria, R. & Jung, R., 1997. An attempt towards a conceptual model derived from 1993−1996 hydraulic operations at Soultz, in *Proceedings of NEDO International Symposium,* Sendai, Japan, Vol. **2,** pp. 329–341.

Giardini, D., 2009. Geothermal quake risks must be faced, *Nature,* **462**(7275), 848–849.

Goebel, T. H. & Brodsky, E. E., 2018. The spatial footprint of injection wells in a global compilation of induced earthquake sequences, *Science,* **361**(6405), 899–904.

Goebel, T. H., Hosseini, S. M., Cappa, F., Hauksson, E., Ampuero, J. P., Aminzadeh, F. & Saleeby, J. B., 2016. Wastewater disposal and earthquake swarm activity at the southern end of the Central Valley, California, *Geophys. Res. Lett.,* **43**(3), 1092–1099.

Goertz-Allmann, B. P., Goertz, A. & Wiemer, S., 2011. Stress drop variations of induced earthquakes at the Basel geothermal site, *Geophys. Res. Lett.,* **38**(9), doi:10.1029/2011GL047498.

Goodfellow, S. D., Nasseri, M. H. B., Maxwell, S. C. & Young, R. P., 2015. Hydraulic fracture energy budget: insights from the laboratory, *Geophys. Res. Lett.,* **42**(9), 3179–3187.

Gualandi, A., Nichele, C., Serpelloni, E., Chiaraluce, L., Anderlini, L., Latorre, D. & Avouac, J. P., 2017. Aseismic deformation associated with an earthquake swarm in the northern Apennines (Italy), *Geophys. Res. Lett.,* **44**(15), 7706–7714.

Guglielmi, Y., Cappa, F., Avouac, J. P., Henry, P. & Elsworth, D., 2015. Seismicity triggered by fluid injection–induced aseismic slip, *Science,* **348**(6240), 1224–1226.

Hamiel, Y., Baer, G., Kalindekafe, L., Dombola, K. & Chindandali, P., 2012. Seismic and aseismic slip evolution and deformation associated with the 2009–2010 northern Malawi earthquake swarm, East African Rift, *Geophys. J. Int.,* **191**(3), 898–908.

Hatch, R. L., Abercrombie, R. E., Ruhl, C. J. & Smith, K. D., 2020. Evidence of aseismic and fluid-driven processes in a small complex seismic swarm near Virginia City, Nevada, *Geophys. Res. Lett.,* **47**(4), e2019GL085477, doi:10.1029/2019GL085477.

Herrmann, M., Kraft, T., Tormann, T., Scarabello, L. & Wiemer, S., 2019. A consistent high-resolution catalog of induced seismicity in Basel based on matched filter detection and tailored post-processing, *J. geophys. Res.,* **124**(8), 8449–8477.

Ide, S., 2001. Complex source processes and the interaction of moderate earthquakes during the earthquake swarm in the Hida-Mountains, Japan, 1998, *Tectonophysics,* **334**(1), 35–54.

Jenatton, L., Guiguet, R., Thouvenot, F. & Daix, N., 2007. The 16,000-event 2003–2004 earthquake swarm in Ubaye (French Alps), *J. geophys. Res.,* **112**(B11), doi:10.1029/2006JB004878.

Kraft, T. & Deichmann, N., 2014. High-precision relocation and focal mechanism of the injection-induced seismicity at the Basel EGS, *Geothermics,* **52,** 59–73.

Kwiatek, G., Saarno, T., Ader, T., Bluemle, F., Bohnhoff, M., Chendorain, M. & Wollin, C., 2019. Controlling fluid-induced seismicity during a 6.1-km-deep geothermal stimulation in Finland, *Sci. Adv.,* **5**(5), doi:10.1126/sciadv.aav722.

Li, B. Q., Smith, J. D. & Ross, Z. E., 2021. Basal nucleation and the prevalence of ascending swarms in Long Valley caldera, *Sci. Adv.,* **7**(35), doi:10.1126/sciadv.abi8368.

Lohman, R. B. & McGuire, J. J., 2007. Earthquake swarms driven by aseismic creep in the Salton Trough, California, *J. geophys. Res.,* **112**(B4), doi:10.1029/2006JB004596.

Madariaga, R., 1976. Dynamics of an expanding circular fault, *Bull. seism. Soc. Am.,* **66**(3), 639–666.

Matsuzawa, T., Uchida, N., Igarashi, T., Okada, T. & Hasegawa, A., 2004. Repeating earthquakes and quasi-static slip on the plate boundary east off northern Honshu, Japan, *Earth, Planets Space,* **56**(8), 803–811.

McGarr, A., 1976. Seismic moments and volume changes, *J. geophys. Res.,* **81**(8), 1487–1494.

McGarr, A., 2014. Maximum magnitude earthquakes induced by fluid injection, *J. geophys. Res.,* **119**(2), 1008–1019.

McGarr, A. & Barbour, A. J., 2018. Injection-induced moment release can also be aseismic, *Geophys. Res. Lett.,* **45**(11), 5344–5351.

Parotidis, M., Rothert, E. & Shapiro, S. A., 2003. Pore-pressure diffusion: a possible triggering mechanism for the earthquake swarms 2000 in Vogtland/NW-Bohemia, central Europe, *Geophys. Res. Lett.,* 30(20).

Passarelli, L., Rivalta, E., Jónsson, S., Hensch, M., Metzger, S., Jakobsdóttir, S. S. & Dahm, T., 2018. Scaling and spatial complementarity of tectonic earthquake swarms, *Earth planet. Sci. Lett.,* **482,** 62–70.

Passarelli, L., Selvadurai, P. A., Rivalta, E. & Jónsson, S., 2021. The source scaling and seismic productivity of slow slip transients, *Sci. Adv.,* **7**(32), doi:10.1126/sciadv.abg9718.

Roland, E. & McGuire, J. J., 2009. Earthquake swarms on transform faults, *Geophys. J. Int.,* **178**(3), 1677–1690.

Ross, Z. E. & Cochran, E. S., 2021. Evidence for latent crustal fluid injection transients in Southern California from long-duration earthquake swarms, *Geophys. Res. Lett.,* **48**(12), doi:10.1029/2021GL092465.

Ross, Z. E., Cochran, E. S., Trugman, D. T. & Smith, J. D., 2020. 3D fault architecture controls the dynamism of earthquake swarms, *Science,* **368**(6497), 1357–1361.

Schmittbuhl, J., Lengliné, O., Cornet, F., Cuenot, N. & Genter, A., 2014. Induced seismicity in EGS reservoir: the creep route, *Geother. Ener.,* **2**(1), 1–13.

Scholz, C. H., 2015. On the stress dependence of the earthquake b value, *Geophys. Res. Lett.,* **42**(5), 1399–1402.

Shapiro, S. A., Dinske, C., Langenbruch, C. & Wenzel, F., 2010. Seismogenic index and magnitude probability of earthquakes induced during reservoir fluid stimulations, *Leading Edge,* **29**(3), 304–309.

Shapiro, S. A., Huenges, E. & Borm, G., 1997. Estimating the crust permeability from fluid-injection-induced seismic emission at the KTB site, *Geophys. J. Int.,* **131**(2), F15–F18.

Shelly, D. R. & Hardebeck, J. L., 2019. Illuminating faulting complexity of the 2017 Yellowstone Maple Creek earthquake swarm, *Geophys. Res. Lett.,* **46**(5), 2544–2552.

Shelly, D. R., Hill, D. P., Massin, F., Farrell, J., Smith, R. B. & Taira, T. A., 2013. A fluid-driven earthquake swarm on the margin of the Yellowstone caldera, *J. geophys. Res.,* **118**(9), 4872–4886.

Simon, V., Kraft, T., Diehl, T. & Tormann, T., 2021. Possible precursory slow-slip to two ML∼ 3 mainevents of the diemtigen microearthquake sequence, Switzerland, *Geophys. Res. Lett.,* **48**(19), e2021GL093783.

Uchida, N., 2019. Detection of repeating earthquakes and their application in characterizing slow fault slip, *Prog. Earth planet. Sci.,* **6**(1), 1–21.

Van der Elst, N. J., Page, M. T., Weiser, D. A., Goebel, T. H. & Hosseini, S. M., 2016. Induced earthquake magnitudes are as large as (statistically) expected, *J. geophys. Res.,* **121**(6), 4575–4590.

Wang, L., Kwiatek, G., Rybacki, E., Bohnhoff, M. & Dresen, G., 2020. Injection-induced seismic moment release and laboratory fault slip: implications for fluid-induced seismicity, *Geophys. Res. Lett.,* **47**(22), e2020GL089576, doi:10.1029/2020GL089576.

Wei, S., Avouac, J. P., Hudnut, K. W., Donnellan, A., Parker, J. W., Graves, R. W. & Eneva, M., 2015. The 2012 Brawley swarm triggered by injection-induced aseismic slip, *Earth planet. Sci. Lett.,* **422,** 115–125.

White, R. & McCausland, W., 2016. Volcano-tectonic earthquakes: a new tool for estimating intrusive volumes and forecasting eruptions, *J. Volc. Geotherm. Res.,* **309,** 139–155.

Wynants-Morel, N., Cappa, F., De Barros, L. & Ampuero, J. P., 2020. Stress perturbation from aseismic slip drives the seismic front during fluid injection in a permeable fault, *J. geophys. Res.,* **125**(7), e2019JB019179, doi:10.1029/2019JB019179.

Wyss, M., 1973. Towards a physical understanding of the earthquake frequency distribution, *Geophys. JR Astron. Soc.,* **31**(4), 341–359.

Yang, Y. & Dunham, E. M., 2021. Effect of porosity and permeability evolution on injection-induced aseismic slip, *J. geophys. Res.,* **126**(7), e2020JB021258, doi:10.1029/2020JB021258.

SUPPORTING INFORMATION

Supplementary data are available at *GJI* online.

Text S1. Data sets.

Figure S1. Example of a Gutenberg–Richter law fit, made over the injection-induced sequence of Basel, Switzerland. Red line represents the distribution of events above a given magnitude while blue line represents the fitting made over this distribution while $M > M_c$ and $N > 10$.

Figure S2. Same as Fig. 4, but without the 10^b factor. R^2 in this case is 0.87.

Table S1. representing the eigenvalues obtained for the 3-D distribution of the hypocentres for each sequence, and the ratio of the smallest eigenvalue to the norm of the two others.

Table S2. Uncertainty in the Gutenberg–Richter law fitting.

Table S3. Data sources.

Please note: Oxford University Press is not responsible for the content or functionality of any supporting materials supplied by the authors. Any queries (other than missing material) should be directed to the corresponding author for the paper.